Journal of Hazardous Materials 195 (2011) 405–413

Contents lists available at SciVerse ScienceDirect

Journal of Hazardous Materials

journal homepage: www.elsevier.com/locate/jhazmat

Treatment of airborne asbestos and asbestos-like microfiber particles using atmospheric microwave air plasma

A. Averroes[a,*], H. Sekiguchi[a], K. Sakamoto[b]

[a] Department of Chemical Engineering, Tokyo Institute of Technology, 2-12-1 O-okayama, Meguro-ku, Tokyo 152-8552, Japan
[b] Street Design Corporation, 6-9-30 Shimo odanaka, Kawasaki-shi, Kanagawa 211-0041, Japan

ARTICLE INFO

Article history:
Received 24 May 2011
Received in revised form 20 August 2011
Accepted 22 August 2011
Available online 27 August 2011

Keywords:
Fiber particle
Airborne asbestos
Microwave air plasma
Atmospheric non-equilibrium plasma
Particle shape index

ABSTRACT

Atmospheric microwave air plasma was used to treat asbestos-like microfiber particles that had two types of ceramic fiber and one type of stainless fiber. The treated particles were characterized via scanning electron microscopy (SEM) and X-ray diffraction (XRD). The experiment results showed that one type of ceramic fiber (Alumina:Silica = 1:1) and the stainless fiber were spheroidized, but the other type of ceramic fiber (Alumina:Silica = 7:3) was not. The conversion of the fibers was investigated by calculating the equivalent diameter, the aspect ratio, and the fiber content ratio. The fiber content ratio in various conditions showed values near zero. The relationship between the normalized fiber vanishing rate and the energy needed to melt the particles completely per unit surface area of projected particles, which is defined as η, was examined and seen to indicate that the normalized fiber vanishing rate decreased rapidly with the increase in η. Finally, some preliminary experiments for pure asbestos were conducted, and the analysis via XRD and phase-contrast microscopy (PCM) showed the availability of the plasma treatment.

1. Introduction

Asbestos refers to natural fibrous silicate minerals with several types based on their composition. They fall into two groups: serpentines and amphiboles [1]. Serpentines are structured with sheets of silicates and essentially consist of chrysotile. Amphiboles have a structure with double-chain silicates such as amosite, crocidolite, and anthophyllite [2]. Asbestos minerals show several good performance aspects such as incombustibility, low thermal conductivity, high electrical resistance, and resistance to alkali, acid, and microorganisms. Because of such properties, asbestos has been widely used in construction.

Asbestos, however, has serious problems such as its needle shape, lightweight, and easy inhalation. When accumulated in the lungs, it is considered to induce two kinds of cancer – mesothelioma and lung cancer – and two nonmalignant conditions: asbestosis and diffuse pleural thickening [3]. Because of these toxicities, the import and fabrication, and use of asbestos have been banned, except for limited uses under the Labor Safety Law Enforcement Ordinance No. 9 since October 1, 2004. The total amount of asbestos imported to Japan until 2004 was about 10 billion tons, 90% of which was used in construction [4]. Therefore, much asbestos can still be expected from the renovation of old buildings that contain asbestos. Some processes aimed at achieving full crystallochemical transformation of asbestos have been studied such as vitrification (1200–1600 °C), ceramization (700–1000 °C), and chemical attack (~50 °C) [1,5,6]. These processes have led to the stabilization of asbestos.

Airborne asbestos is very harmful, and a person leaving a disposal station for asbestos-containing materials needs efficient treatment. Therefore, this study proposes the treatment of airborne asbestos from the exhaust gas of disposal stations with microwave air plasma to prevent its spread.

Microwave plasma is an electrical discharge with microwave as its source energy. It has some advantageous features such as electrode-less discharge, high gas temperature (about 3000 °C), and compact size [7]. Its electrode-less discharge enables it to be unaffected by oxygen. The apparatus has almost the same size as a kitchen microwave oven, so it can be easily attached to the disposal station. Moreover, it is possible to convert air into stable plasma with a small amount of electricity. Applying this high gas temperature will melt asbestos and then spheroidize it and change its composition. Thus, the hazard of asbestos is deemed to be decreased.

In this study, atmospheric microwave air plasma treatment of asbestos-like microfiber materials was investigated under several experiment conditions. These microfiber materials were chosen because they have similar needle shaped and close melting points to asbestos. The plasma-treated fiber materials were observed with scanning electron microscopy (SEM). The diameter of the

* Corresponding author. Tel.: +81 3 5734 2110.
E-mail address: aulia.a.aa@m.titech.ac.jp (A. Averroes).

0304-3894/$ – see front matter © 2011 Elsevier B.V. All rights reserved.
doi:10.1016/j.jhazmat.2011.08.062

Nomenclature

S	area of the projected particle (m^2)
D_a	diameter of the equivalent circular area (m)
W	minor axis of the approximate ellipse of the projected particle (m)
L	major axis of the approximate ellipse of the projected particle (m)
AR	aspect ratio (−)
V	fiber content ratio (−)
t_1	time required to increase the temperature of the particle until its melting point (s)
t_2	time required to melt the particle completely at its melting point (s)
h	heat transfer coefficient of plasma ($W\,m^{-2}\,K^{-1}$)
ρ_p	density of the solid particle ($kg\,m^{-3}$)
V_p	volume of the solid particle (m^3)
A_p	surface area of the solid particle (m^2)
λ	melting heat of the solid particle ($J\,kg^{-1}$)
C_p	specific heat ($J\,kg^{-1}\,K^{-1}$)
k	thermal conductivity of plasma ($W\,m^{-1}\,K^{-1}$)
D_p	diameter of the solid particle (m)
T_f	temperature of plasma (K)
T_0	initial temperature of the particle (K)
T_m	melting point of the particle (K)
$-\Delta V$	fiber vanishing rate (−)
$-\Delta V/V_0$	normalized fiber vanishing rate (−)

equivalent circular area, the aspect ratio, and the fiber content ratio were used as particle shape indices. The relationship between the heat needed to melt the particle per surface area and the fiber vanishing rate were also considered in evaluating the applicability of the plasma method. Once the methodology was optimized, three types of pure asbestos were plasma-treated, and the content of the asbestos after its plasma treatment was evaluated.

2. Experiment

2.1. Experimental methodology

Fig. 1 shows the experimental setup of the plasma treatment. To generate plasma, air streams were fed tangentially through a nozzle into a quartz torch (I.D.: 9.5 mm). Microwave power (2.45 GHz, maximum power 1.5 kW, IDX Co., Ltd.) was coupled to the gas as it passed through a rectangular waveguide. Pure argon gas was introduced for the plasma ignition before creating totally pure air plasma.

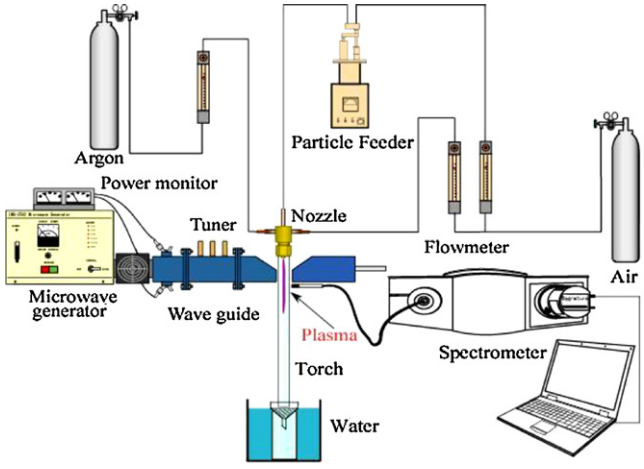

Fig. 1. Experiment apparatus.

Table 1
Experiment conditions.

Reaction tube (mm)	I.D. = 9.5, O.D. = 11.6, L = 400
Swirl air flow rate (L/min)	8.1, 11.4, 14.0
Carrier gas flow rate (L/min)	3.5, 5.1
Input power (W)	1000
Type of fiber particle:	
IBI wool (IW)	Al_2O_3 = 0.46, SiO_2 = 0.51
SMF300UE (SMF)	Fe = 0.83, Cr = 0.16, Ferritic stainless steel = 0.01
Fibermax (FM)	Al_2O_3 = 0.72, SiO_2 = 0.28
Pure chrysotile (CHR)	$Mg_3Si_2O_5(OH)_4$ = 0.95
Pure amosite (AMO)	$(Fe,Mg)_7(Si_8O_{22})(OH)_2$ = 0.99
Pure crocidolite (CRO)	$Na_2Fe_3^{2+}Fe_2^{3+}(Si_8O_{22})(OH)_2$ = 0.99
Particle density (kg/m^3)	IW = 2700; SMF = 7700; FM = 2900
	CHR = 2550; AMO = 3475
	CRO = 3250
Melting point (K)	IW = 2033; SMF = 1742; FM = 2143
	CHR = 1794; AMO = 1572; CRO = 1466
Melting enthalpy (kJ/mol)	IW = 436; SMF = 272; FM = 588
	CHR = 1012; AMO = 359; CRO = 529
Fiber average diameter (μm)	IW = 1.8–3, SMF = 5–10, FM = 4–6
	CHR = 25.5, AMO = 24, CRO = 29
Fiber average length (μm)	IW = 34, SMF = 15–50, FM = 48
	CHR = 53, AMO = 96, CRO = 98.5

Raw particles were fed constantly into the air plasma from the top of the quartz tube with a particle feeder (type: MF, Technoserve Co., Ltd.) and air as a carrier gas. The plasma-treated particles were trapped in water and filtered. Then the samples were dried and analyzed via SEM (KEYENCE, VE-8800) to observe their melting condition and shape change. They were also analyzed via X-ray diffraction (RIGAKU, RINT-2200) to investigate their phase alteration. Three kinds of microfiber particles were used as precursor materials: IBI wool (IW, Ibiden Co.); stainless fiber (SMF300UE, JFE Techno-research Co.); and Fibermax (FM, ITM Co.). The experiment was conducted by varying the particle feed rate and the swirl air gas flow rate, which are the experiment conditions listed in Table 1.

Once the methodology was optimized, experiment results on pure asbestos of the Japan Association for Working Environment Measurement (JAWE) were described. Due to the handling of hazardous materials, the experiments were conducted in an area cleared by the Ministry of Environment of Japan. The layout of the workplace is shown in Fig. 2. It was isolated with a double plastic sheet. A Negative Air Machine with HEPA filter was used as an air ventilator. A security zone was set at the entrance that was equipped with an air shower machine. Safety equipment such as dust masks, coveralls, gloves, and shoe covers were provided to prevent exposure to airborne asbestos while undressing in the workplace.

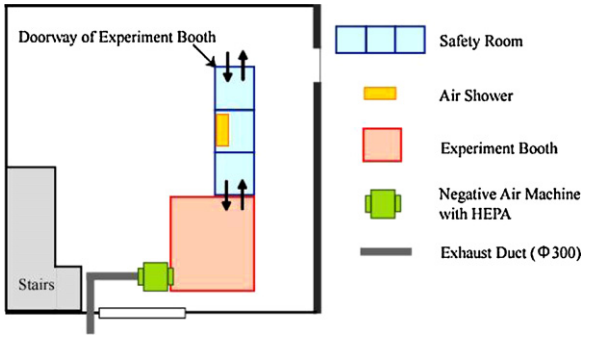

Fig. 2. Layout of the workplace.

Table 2
Average values of particle shape indices before treatment.

Type of fiber particle	IBI wool	SMF300UE	Fibermax	Pure chrysotile	Pure amosite	Pure crocidolite
D_a [μm]	16.7	25.0	17.4	35.8	42.9	48.1
AR [−]	0.32	0.43	0.19	0.485	0.25	0.29

2.2. Two-dimensional analysis

100–200 samples of both the treated and untreated particles were captured via SEM, after which an image analysis software (Scion Image) was used to measure the area of the projected particle (S) and the major axis (L) and minor axis (W) of an approximate ellipse of the projected particle. The diameter of the equivalent circular area (D_a) and the aspect ratio (AR) were used as the particle shape indices [Eqs. (1) and (2)], with the initial values shown in Table 2. The diameter of the equivalent circular area was determined using Eq. (1), from the diameter of a circle that had the same area as the projected particle. The aspect ratio (AR) shows the ratio of the major axis to the minor axis of an approximate ellipse of the projected particles, as shown in Eq. (2).

$$D_a = 2\sqrt{\frac{S}{\pi}} \tag{1}$$

$$\mathrm{AR} = \frac{W}{L} \tag{2}$$

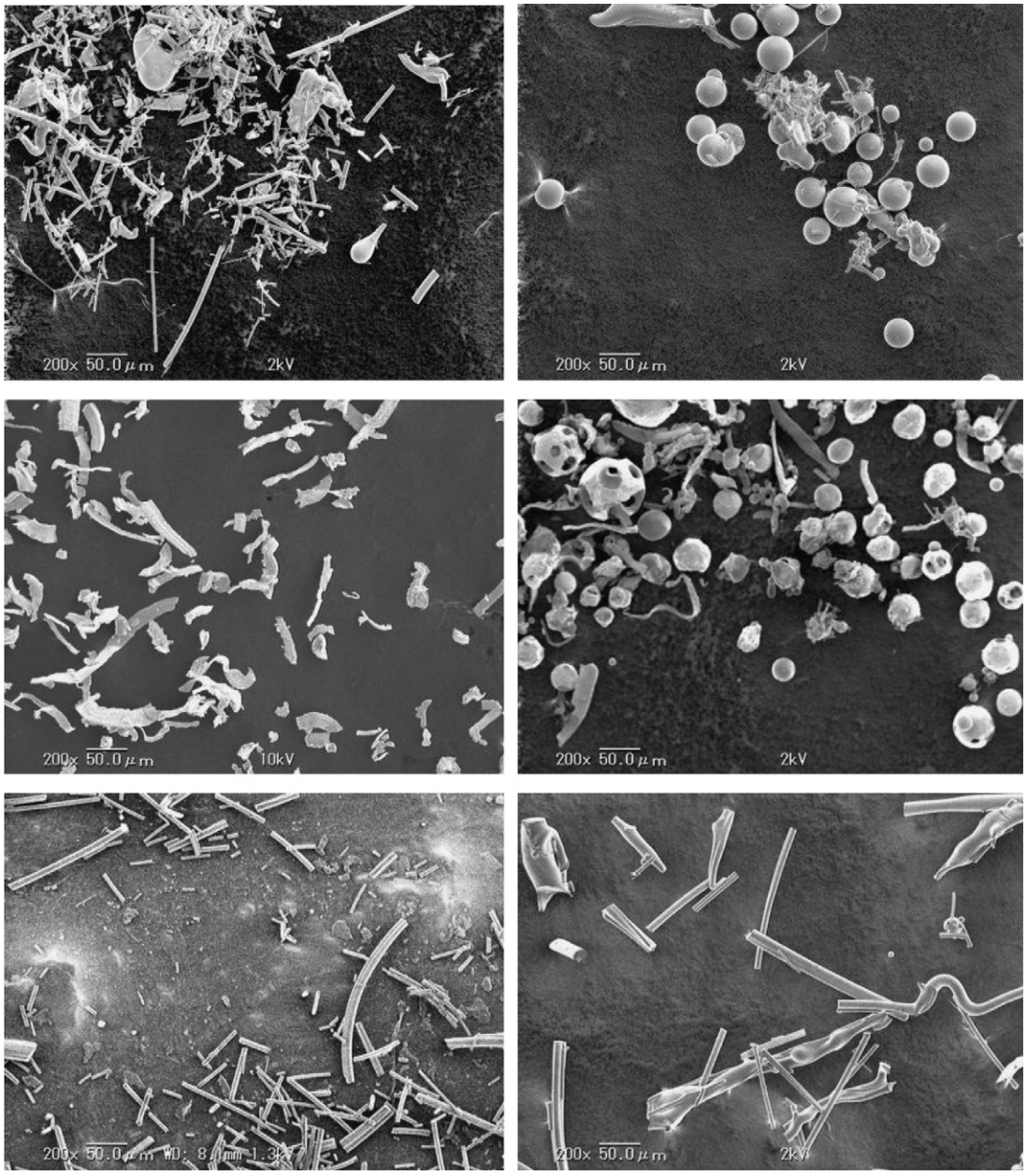

Fig. 3. SEM photographs of the microfiber particles before (left) and after (right) their air plasma treatment for IBI wool (top), SMF300-UE (center), and Fibermax (bottom).

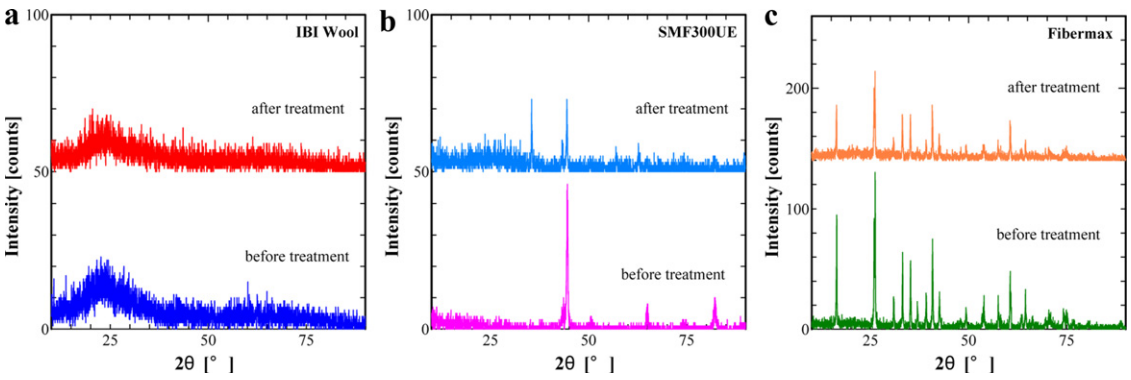

Fig. 4. XRD patterns of the microfiber particles before and after their treatment for (a) IBI wool, (b) SMF300UE, and (c) Fibermax.

3. Results

3.1. Treatment of the microfiber particles

3.1.1. Change in the shape of the particles after their plasma treatment

Fig. 3 shows the SEM pictures of the microfiber particles before and after their plasma treatment at 1 kW microwave power, a 11.4 L/min swirl air flow rate, and a 3.5 L/min carrier gas flow rate. At 200× magnification, all three types of microfiber particles contained many fibrous particles before their plasma treatment. Moreover, there was no spherical particle in the untreated microfiber, but many spherical particles emerged from the treated fiber particles, except for Fibermax. Under several experiment conditions, the spheroidized particles were mixed with the agglomerated and unconverted particles.

3.1.2. Investigation by X-ray diffraction

XRD analysis of both the untreated and treated microfiber particles was conducted to detect the phase change after the treatment (Fig. 4). IBI wool and Fibermax showed no alteration in their phases, which showed the typical peaks of amorphous ceramic fiber and mullite fiber, respectively. The SMF300UE of the stainless fiber had different peaks before and after its plasma treatment, though. The peaks describe the X-ray diffraction (XRD) pattern of the ferrite stainless steel ($2\theta = 44.6$, 64.93, and 82.1) for the particles before the treatment [8], but the peaks of chromite and/or magnetite ($2\theta = 35.5$) appeared after the treatment [9]. It can thus be said that the phase change occurred during the plasma treatment of the stainless fiber.

3.1.3. Effects of the particle feed rate on the particle shape indices

The particle shape indices were used to investigate the results of the plasma treatment. The difference between the particle shape indices before and after the treatment was calculated and described with a delta (Δ). The effects of the particle feed rate on the average difference in the equivalent diameter and the difference in the aspect ratio are shown in Fig. 5(a) and (b) at a 1 kW input power and a 11.1 L/min air flow rate, with the values at point zero indicating the conditions before the treatment. In the case of IBI wool, ΔD_a had a large value at a small particle feed rate, then decreased and tended to be constant with the increase in the particle feed rate. ΔD_a seems to have had a peak with the increase in the particle feed rate for SMF300UE and Fibermax. Actually, due to the high standard deviation, the tendency that appeared was weak. Although, this could have indicated that almost all the particles were agglomerated since almost of ΔD_a was greater than zero. This is important because the bigger size will decrease the harmful effect of fiber. It showed, however, that ΔAR had a different tendency for all types of microfiber particles. The average ΔAR of IBI wool was 0.4 and tended to remain constant, and the values of both SMF300UE and Fibermax tended to decrease as the particle feed rate increased.

3.1.4. Effects of the swirl air flow rate on the particle shape indices

Fig. 6(a) and (b) shows the behavior of the average difference in the equivalent diameter and the difference in the aspect ratio at the swirl air flow rates of 8 L/min, 11.1 L/min, and 14 L/min. As the

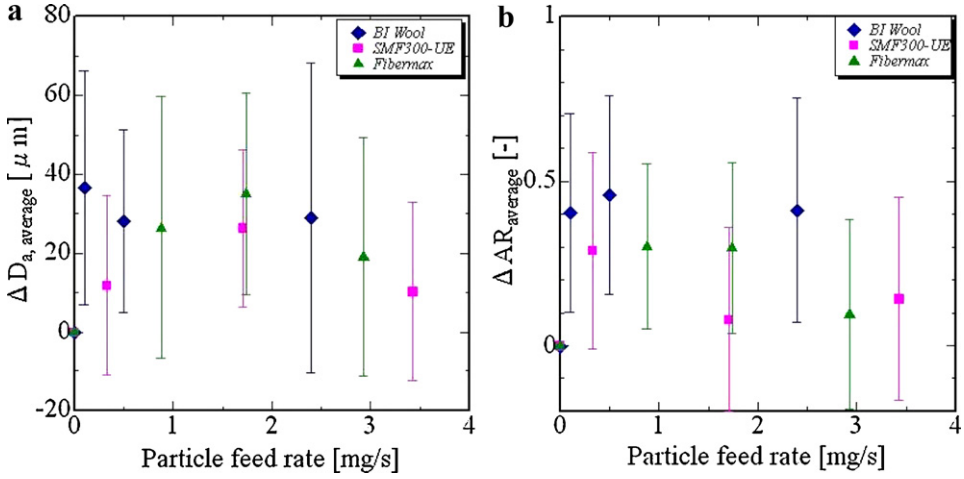

Fig. 5. Effects of the particle feed rate on the (a) equivalent diameter and (b) average aspect ratio for an input power of 1000 W and a swirl air flow rate of 11.1 L/min).

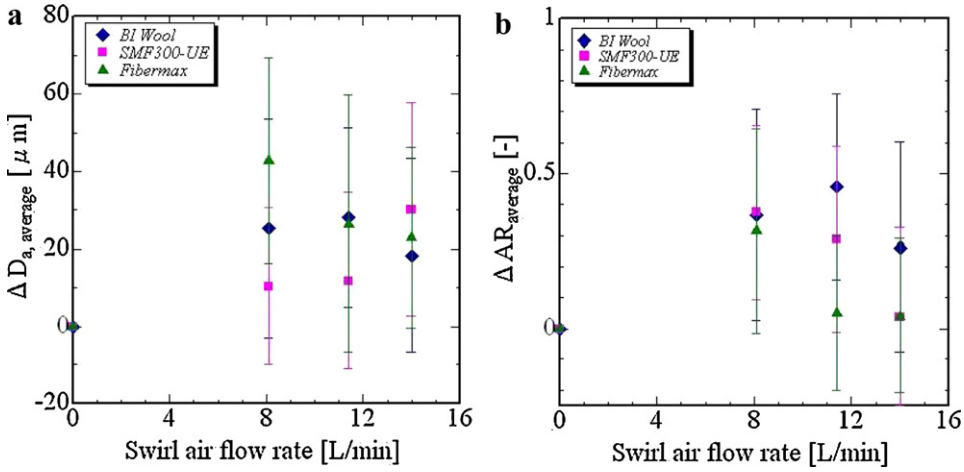

Fig. 6. Effects of the swirl air flow rate on the (a) equivalent diameter and (b) average aspect ratio for an input power of 1000 W and a carrier gas flow rate of 3.5 L/min.

swirl air flow rate increased, the average ΔD_a decreased for IBI wool and Fibermax, but not for SMF300UE. This is interesting because the volume of plasma is considered to be lower at a higher swirl air flow rate [9], which should result in a lower melting condition. The average ΔD_a of SMF300UE peaked at 14.0 L/min, though. This suggests that at this rate, the fiber particles of SMF300UE received a higher gravity force due to their density and tended to have a short transit time inside the plasma. As a result, SMF300UE melted only at the surface, attached to each other, and agglomerated to form a bigger size.

On the other hand, the average ΔAR indicates the lowest point for all types of microfiber particles at a swirl air flow of 14.0 L/min, as shown in Fig. 5(b), which was a reasonable result because the volume of the plasma plume was considered to have been lowest at that condition [10]. Thus, fewer particles passed through the high-temperature plasma region.

The arithmetic average of the aforementioned ΔD_a and ΔAR has a wide standard deviation that makes it difficult to clearly conclude the tendency of the treatment results. By assuming, however, that each case had a normal distribution, the amount of particles left untreated was predicted.

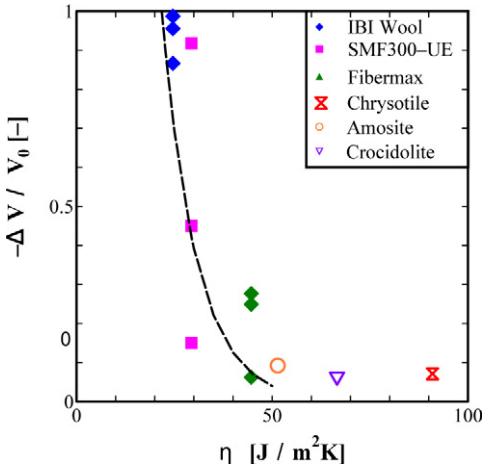

Fig. 8. Relationship between η and the normalized fiber vanishing rate ($-\Delta V/V_0$) of (a) the microfiber particle only (IP = 1000 W and AFR = 11.4 L/min) and (b) of the microfiber particle with pure asbestos (IP = 1000 W and AFR = 12.5 L/min).

3.1.5. Adoption of the fiber content rate

As noted in the previous section, it was difficult to clearly conclude the results tendency using the arithmetic average. Besides, the average value often fails to express the real conditions with respect to energy. Even if two particles have the same aspect ratio, the bigger particle needs more heat to melt. The arithmetic average is still important from the aspect of safety. According to the World Health Organization (WHO), asbestos fiber has an aspect ratio that is greater than 3:1 [11]. Based on this, the fiber content ratio is

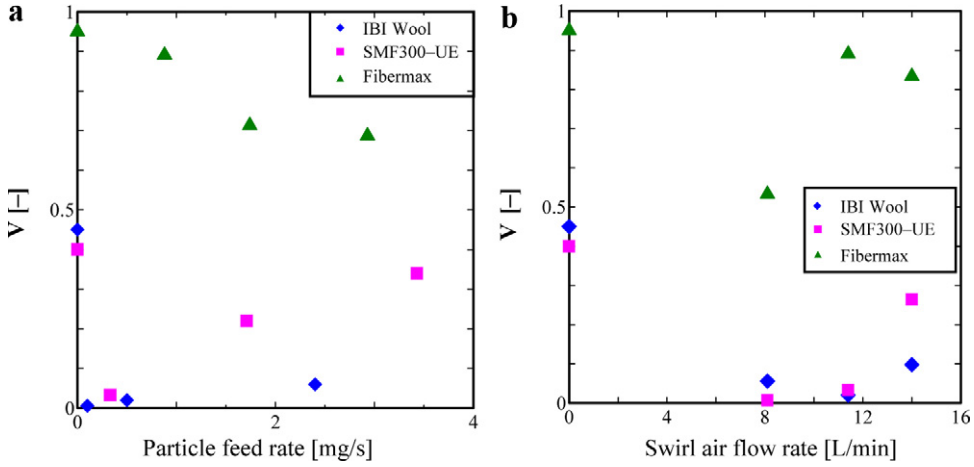

Fig. 7. Behavior of the fiber content rate for an input power of 1000 W due to the change in the (a) particle feed rate and (b) swirl air flow rate.

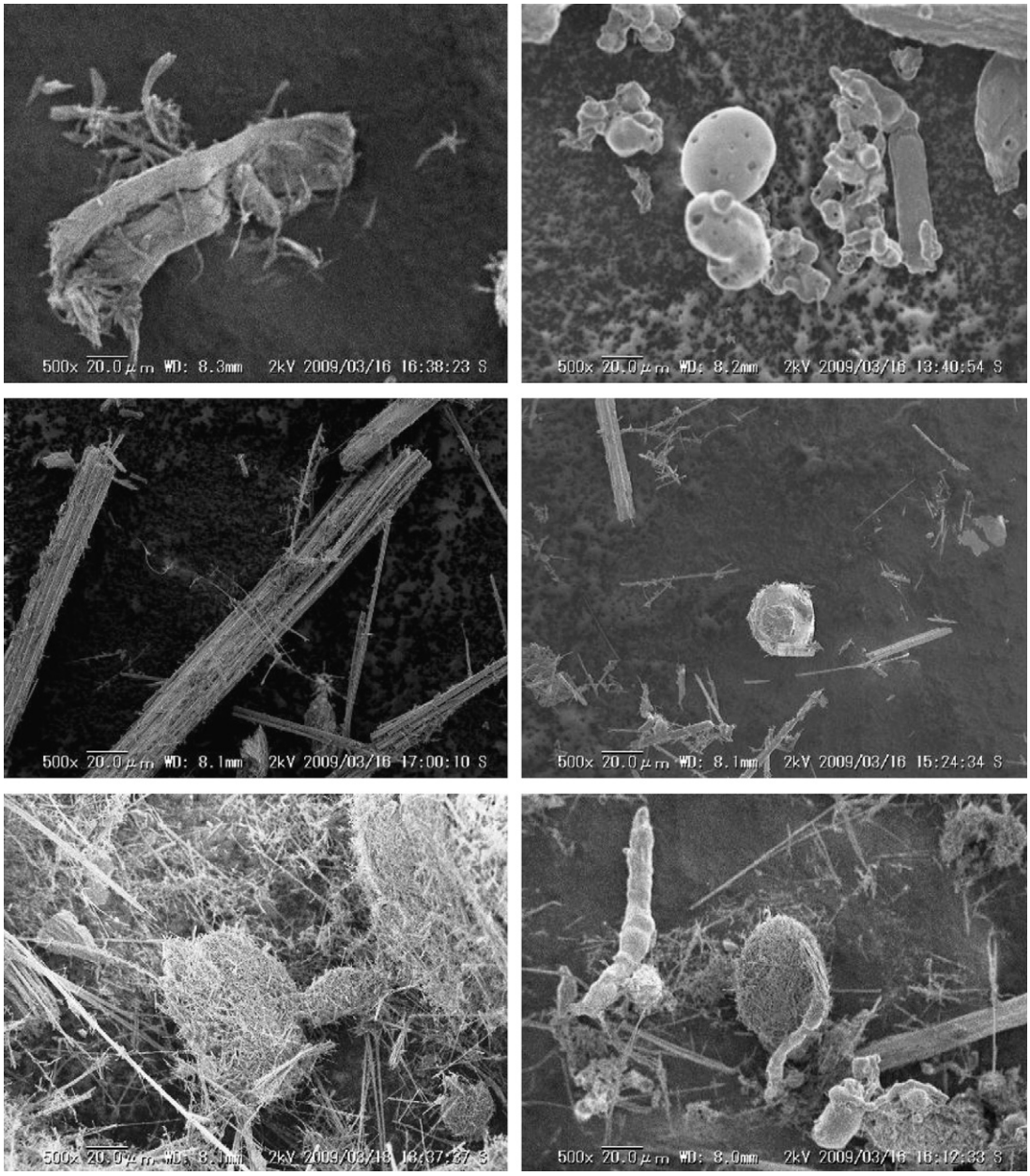

Fig. 9. SEM photographs of the pure asbestos before (left) and after (right) its air plasma treatment for chrysotile (top), amosite (center), and crocidolite (bottom).

defined as the ratio of the projected area of the particles with an AR value below 0.33 to the total area of the projected particles, as follows.

$$V = \frac{\sum \text{projected area of particle with AR} \leq 0.33}{\sum \text{projected area of particle}} \times 100\% \quad (3)$$

The effects of the particle feed rate and the swirl air flow rate on the fiber content ratio are shown in Fig. 7. The values at zero on the x axis represent the fiber content ratio of the microfiber particles before the plasma treatment. The fiber content ratio of IBI wool and SMF300UE decreased to almost zero at a lower particle feed rate and a lower swirl air flow rate. The fiber content ratio of Fibermax decreased only to about 0.7 for the experiments with the particle feed rate as a parameter and to 0.5 at the lowest value of the swirl air flow rate. By adopting this new particle shape index, it can be concluded that IBI wool and SMF300UE were better treated than Fibermax and showed an approximately zero value for the fiber content ratio under several experiment conditions. These results indicate that this method would be useful for asbestos, the melting point of which is roughly similar to that of these microfibers.

3.1.6. Heat transfer between the plasma and the fiber particle

Although the fiber content ratio can describe the tendency of the results under each experiment condition, the particle shape index, which can evaluate the potential of this method, is necessary.

In this section, the heat balance between the plasma and the microfiber particles is discussed. The mechanism of the plasma treatment can be described as follows. First, the particles receive heat from the plasma and melt instantaneously, and then the melted particles rapidly cool at the plasma afterglow. Thus, by assuming that there is no temperature gradient inside the

particle and that the effect of radiation can be neglected, the complete melting time is described in Eq. (4).

$$t_1 + t_2 = \frac{1}{h}\left[\frac{\rho V_p C_p}{A_p}\ln\left(\frac{T_f - T_0}{T_f - T_m}\right) + \frac{\rho V_p \lambda}{A_p(T_f - T_m)}\right] \quad (4)$$

$$h(t_1 + t_2) = \frac{\rho V_p C_p}{A_p}\ln\left(\frac{T_f - T_0}{T_f - T_m}\right) + \frac{\rho V_p \lambda}{A_p(T_f - T_m)} = \eta \quad (5)$$

It was assumed that the plasma temperature was 3000 K [12,13] and that all the particles before the treatment were cylindrical. Then the new parameter η in Eq. (5) was introduced and calculated. In the equation, η is the product of the multiplication of the heat coefficient of the plasma and the complete melting time, which indicates the amount of energy needed to melt the particles completely per unit surface area. The relationship between η and the normalized fiber vanishing rate $(-\Delta V/V_0)$ is shown in Fig. 8. The fiber vanishing rate $(-\Delta V)$ is the difference between the fiber content ratio before and after the treatment, and V_0 is the fiber content ratio before the treatment.

As shown in Fig. 8, the normalized fiber vanishing rate had a downward tendency with an increase in η, which has a rational tendency. The same experiment conditions brought about nearly the same normalized fiber vanishing rate. Thus, the fiber vanishing rate is suggested as a proper index for evaluating the result of this treatment method.

By assuming that the correlation in Fig. 8 is valid, an approximate curve line can be drawn, and it becomes possible to estimate the value of η that makes $-\Delta V/V_0$ equal to unity. Moreover, by introducing the natures of pure asbestos in Eq. (5), the normalized fiber vanishing rate is expected to reach unity for a cylinder diameter equal to or less than 10 μm. Actually, it is still necessary to verify this relationship by calculating a numerical model.

4. Prove treatment of pure asbestos

4.1. SEM analysis of the plasma treatment of pure asbestos

Fig. 9 shows SEM pictures of the pure asbestos before and after its plasma treatment at 1 kW input power, a 12.5 L/min swirl air flow rate, and a 2.5–5.3 L/min carrier gas flow rate. At 500× magnification, some fibers were still observed in amosite and crocidolite, but not in chrysotile, as shown in Fig. 8. The bigger size of the plasma-treated particles indicates the agglomeration of the particles during the treatment.

4.2. Investigation of the plasma content in the plasma-treated pure asbestos

To determine the effects of plasma treatment of pure asbestos, the XRD patterns of the pure asbestos after the treatment were compared with the XRD patterns before the treatment (Fig. 10). Asbestos has some typical peaks that represent its content. Asbestos peaks (chrysotile = 12 and 24; amosite = 10.7, 27.3, and 29.1; and crocidolite = 10.5, 28.6, and 32.8) were confirmed for all the untreated pure asbestos samples. The peaks of chrysotile mostly disappeared after its treatment and new crystalline peaks of forsterite (2θ = 17.4, 23 and 32.4) and enstatite (2θ = 31) appeared. The formation of forsterite and enstatite will occur as chrysotile heated more than 850 °C [14,15]. However, the typical peaks of amosite and crocidolite remained, though they significantly decreased. In the case of amosite, the formation of oxy-amosite occurs at relatively low temperature (~500 °C). The breakdown of oxy-amosite begins at = 800 °C produces the decomposition of hematite, magnetite, and possibly quartz [15]. Some new peaks of α-quartz (2θ =21 and 27) and magnetite (2θ = 18) appeared as

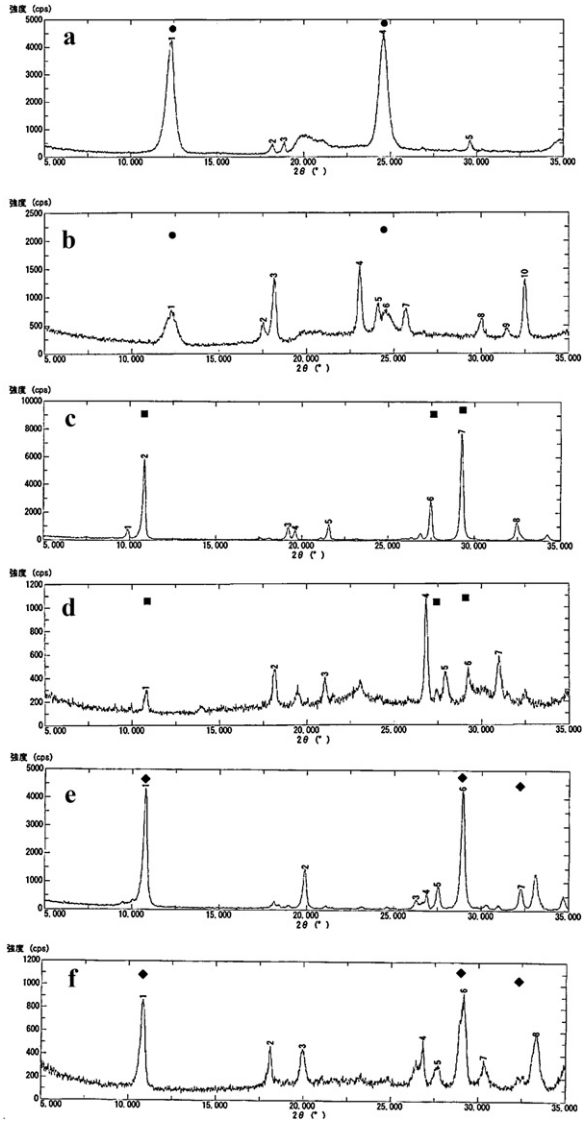

Fig. 10. XRD patterns of the pure asbestos before its plasma treatment for (a) chrysotile, (c) amosite, and (e) crocidolite; and after its treatment for (b) chrysotile, (d) amosite, and (f) crocidolite. ●, chrysotile; ■, amosite; □, crocidolite.

shown in Fig. 10(d). For transformation of crocidolite, the formation of oxy-crocidolite occurs at temperatures up to 650 °C. Above 650 °C the oxy-crocidolite begins to break down with formation of acmite, hematite, cristobalite, and possibly some magnetite [15]. Some new peaks of acmite (2θ = 30), hematite (2θ = 33), and magnetite (2θ = 18) were detected after treatment as shown in Fig. 10(f).

The plasma-treated pure asbestos was analyzed with phase-contrast polarized light microscopy to confirm the results of the XRD analysis. This was because XRD cannot distinguish between asbestiform and nonasbestiform materials with the same mineral phase [16]. This is why the qualitative analysis of asbestos via XRD must be confirmed via either phase-contrast microscopy (PCM) or SEM.

Actually, the dispersion staining methods of light microscopy can uniquely identify asbestos fibers with diameters as small as 1 μ m. This technique involves suspending liquids of known refractive indices (Cargille refractive index liquids) and observing their color display by means of a dispersion staining objective [17]. Asbestos minerals have double refractive indices. By immersing the fiber in appropriate liquids, the optical properties of asbestos signals can be detected from a unique color combination with

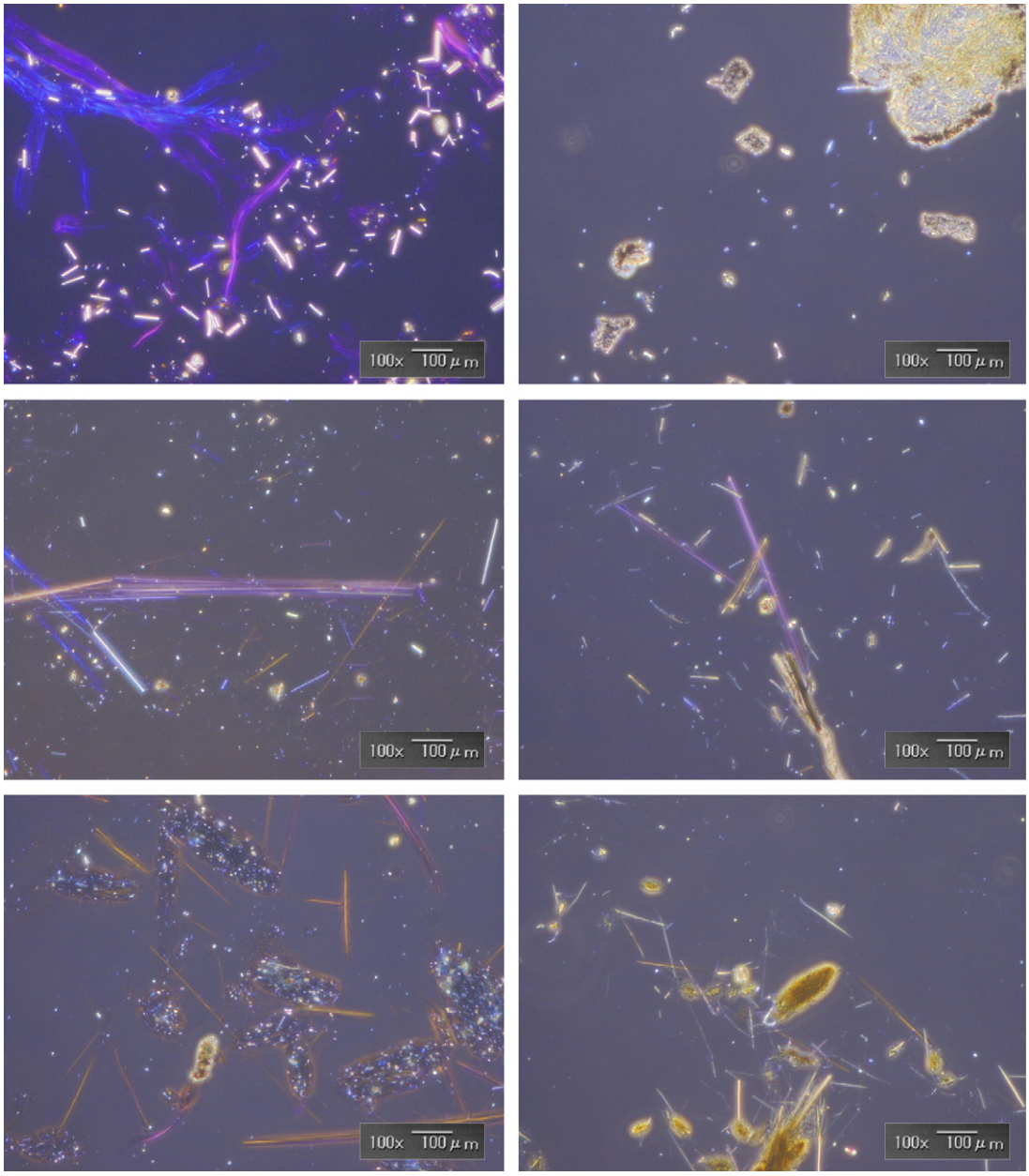

Fig. 11. Pictures from a phase-contrast microscope (100×) of the pure asbestos before its treatment (left) and after its treatment (right) for chrysotile (top), amosite (center), and crocidolite (bottom).

the polarized light. This identification was conducted via phase-contrast microscopy (Nikon, Eclipse 80i) on pure asbestos before and after the treatment. The asbestos dispersion-staining colors (chrysotile = blue-violet, amosite = peach, and crocidolite = orange) for the particles after the treatment were not detected, as shown in Fig. 11, unlike the particles before the treatment.

From the aforementioned results, asbestos peaks were detected via XRD but were undetected via PCM. Many needle-shaped particles remained in the treated particles of amosite and crocidolite which was suggested due to the cohesion of pure asbestos particles, especially for amosite and crocidolite. This somehow causes bunch formation of the fiber particles, which affects their steady feeding. This condition affected the temperature of the air plasma when many particles were fed into the quartz tube in one burst.

Moreover, referring to Fig. 8 in Section 3.1.6, the value of the normalized fiber vanishing rate of the pure asbestos is small. It can be considered that the experiment results for pure asbestos did not reach unity because its fiber structure formed a bunch shape that increased its average diameter to more than 10 μm, as shown in Table 1. Pure asbestos is practically never used, however, and airborne asbestos is usually dispersed in the air, with a smaller diameter of about 1–2 μm [18].

5. Conclusion

Atmospheric microwave air plasma was used to treat microfiber particles, followed by the conduct of the prove test for pure asbestos-containing materials by altering the particle feed rate and the swirl air flow rate as the experiment parameters. The SEM results showed that the plasma-treated microfiber particles were spheroidized and agglomerated. The XRD analysis results showed that the peaks of the pure amosite and the pure crocidolite remained, but not that of the pure chrysotile. The PCM results indicated, however, that there was no asbestos in the plasma-treated

pure asbestos particle. Therefore, this method was shown to be suited for pure chrysotile and needs some improvement especially for pure amosite and pure crocidolite.

Regarding energy use, the fiber content ratio and the fiber vanishing rate were used as the particle shape indices. A rational correlation between the amount of energy needed per unit surface area (η) and the normalized fiber vanishing rate was observed. Finally, it is suggested that this atmospheric microwave air plasma treatment method has potential for the treatment of airborne building materials that contain asbestos. That means this technology will be efficient to treat airborne asbestos that contained in exhaust gas of asbestos disposal station. Airborne building materials such as cement and concrete will also be treated due to the high temperature of plasma.

Acknowledgments

The authors are grateful to the Ministry of Education, Culture, Sports, Science, and Technology of Japan, and to the Japan Science and Technology Agency, for their financial support for this research.

References

[1] F. Turci, M. Tomatis, S. Mantegna, G. Cravotto, B. Fubini, A new approach to the decontamination of asbestos-polluted waters by treatment with oxalic acid under power ultrasound, Ultrason. Sonochem. 15 (2008) 420–427.
[2] C. Leonelli, P. Veronesi, D.N. Boccaccini, M.R. Rivasi, L. Barbieri, F. Andreola, I. Lancellotti, D. Rabitti, G.C. Pellacani, Microwave thermal inertisation of asbestos containing waste and its recycling in traditional ceramics, J. Hazard. Mater. B 135 (2006) 149–155.
[3] A.J. Darnton, D.M. McElvenny, J.T. Hodgson, Estimating the number of asbestos-related lung cancer death in Great Britain from 1980 to 2000, Ann. Occup. Hyg. 50 (2006) 29–38.
[4] M. Fujishige, R. Sato, A. Kuribara, I. Karasawa, A. Kojima, Low-temperature decomposition of sprayed-on asbestos, J. Ceram. Soc. Jpn. 114 (2006) 1133–1137.
[5] P. Plescia, D. Gizzi, S. Benedetti, L. Camilucci, C. Fanizza, P.D. Simone, F. Paglietti, Mechanochemical Treatment to recycling asbestos-containing waste, Waste Manage. 23 (2002) 209–218.
[6] E. Gomez, D. Amutha Rani, C.R. Cheeseman, D. Deegan, M. Wise, A.R. Boccaccini, Thermal plasma technology for the treatment of wastes: a critical review, J. Hazard. Mater. 161 (2009) 614–626.
[7] S. Nakanishi, H. Sekiguchi, Comparison of reforming behaviors of hexane and isooctane in microwave steam plasma, J. Jpn. Petrol. Inst. 48 (2005) 22–28.
[8] H. Tsujimura, T. Goto, Y. Ito, Electrochemical surface nitriding of SUS 430 ferritic stainless steel, Mater. Sci. Eng. A355 (2003) 315–319.
[9] D. Majuste, M.B. Mansur, Leaching of the fine fraction of the argon oxygen decarburization with lance (AOD-L) sludge for the prefential removal of iron, J. Hazard. Mater. 162 (2009) 356–364.
[10] K.M. Green, M.C. Borras, P.P. Woskov, G.J. Flores, K. Hadidi, P. Thomas, Electronic excitation temperature profiles in an air microwave plasma torch, IEEE Trans. Plasma Sci. 29 (2001) 399–406.
[11] K. Donaldson, C.L. Tran, An introduction to the short-term toxicology of respirable industrial fibres, Mutat. Res. 553 (2004) 5–9.
[12] S.Y. Moon, W. Choe, Parametric study of atmospheric pressure microwave-induced Ar/O_2 plasmas and the ambient air effect on the plasma, Phys. Plasmas 13 (2006), 103503:1-6.
[13] J. Happold, P. Lindner, R. Roth, Spatially resolved temperature measurement in an atmospheric plasma torch using the $A^2\Sigma^+$, $v' = 0 \rightarrow X^2\Pi$, $v'' = 0$ OH band, J. Phys. D: Appl. Phys. 39 (2006) 3615–3620.
[14] T. Zaremba, A. KArzakala, J. Piotrowski, D. Garcczorz, Study on the thermal decomposition of chrysotile asbestos, J. Therm. Anal. Calorim. 101 (2010) 479–485.
[15] M. Jeyaratnam, N.G. West, A Study of heat-degraded chrysotile, amosite, and crocidolite by X-ray diffraction, Ann. Occup. Hyg. 38 (1994) 137–148.
[16] D.A. Vallero, M.E. Beard, Selecting appropriate analytical methods to characterize asbestos in various media, the practice periodical of hazardous, toxic, and radioactive, Waste Manage. 13 (2009) 249–260.
[17] W.C. McCrone, Detection and Identification of asbestos by microscopical dispersion staining, Environ. Health Perspect. 9 (1974) 57–61.
[18] S. Hashimoto, H. Takeda, A. Okuda, A. Kambayashi, S. Honda, H. Awaji, K. Fukuda, Detoxification of asbestos-containing building material waste and its application to cement product, J. Ceram. Soc. Jpn. 115 (2007) 290–293.